Acta Materialia 232 (2022) 117944

Contents lists available at ScienceDirect

Acta Materialia

journal homepage: www.elsevier.com/locate/actamat

Full length article

Ultralong one-dimensional plastic zone created in aluminum underneath a nanoscale indent

Zhi-Yu Nie[a], Yuji Sato[b], Shigenobu Ogata[c], Maria Jazmin Duarte[d], Gerhard Dehm[d], Ju Li[e], Evan Ma[f], De-Gang Xie[a,*], Zhi-Wei Shan[a,*]

[a] Center for Advancing Materials Performance from the Nanoscale (CAMP-Nano), State Key Laboratory for Mechanical Behavior of Materials, Xi'an Jiaotong University, Xi'an 710049, China
[b] Department of Mechanical Engineering, The University of Tokyo, Tokyo 113-8656, Japan
[c] Department of Mechanical Science and Bioengineering, Osaka University, Osaka 560-8531, Japan
[d] Max-Planck-Institut für Eisenforschung GmbH, Düsseldorf 40237, Germany
[e] Department of Nuclear Science and Engineering and Department of Materials Science and Engineering, Massachusetts Institute of Technology, Cambridge, MA 02139, USA
[f] Center for Alloy Innovation and Design, State Key Laboratory for Mechanical Behavior of Materials, Xi'an Jiaotong University, Xi'an, China

A R T I C L E I N F O

Article history:
Received 11 November 2021
Revised 17 March 2022
Accepted 13 April 2022
Available online 16 April 2022

Keywords:
Nanoindentation
Indentation size effect
Dislocation structure
In situ TEM
Incipient plasticity

A B S T R A C T

Nanoindentation on crystalline materials is generally believed to generate a three-dimensional plastic zone, which has a semi-spherical shape with a diameter no larger than a few times the indentation depth. Here, by observing nanoindentation on aluminum *in situ* inside a transmission electron microscope, we demonstrate that three-dimensional plasticity dominated by regular dislocations triumph as the contact size upon yielding increases above ~100 nm. However, when the contact diameter is less than ~50 nm, a narrow and long (hereafter referred to as "one dimensional") plastic zone can be created in front of the tip, as the indenter successively injects prismatic dislocation loops/helices into the crystal. Interestingly, this one-dimensional plastic zone can penetrate up to 150 times the indentation depth, far beyond the prediction given by the Nix-Gao model. Our findings shed new light on understanding the dislocation behavior during nanoscale contact. The experimental method also provides a potentially novel way to interrogate loop-defect interactions, and to create periodic loop arrays at precise positions for the modification of properties (*e.g.*, strengthening).

1. Introduction

Quantitative mechanical measurements using nanoindentation or atomic force microscopy (AFM) are powerful in probing crystal plasticity at the nanoscale. The displacement burst (or "pop-in") [1–6] offers useful information regarding the nucleation and propagation of dislocations involved in initial yielding. In nanoindentation testing, the stress distribution produced by the indenter is not uniform, with the stress level decreasing rapidly with increasing distance from the local region under the indenter, generating a three-dimensional hemispherical stress field [7]. As a result, the nucleation and propagation of dislocations in the hemispherical region produce a corresponding plastic zone. Such a three-dimensional plastic zone (3D PZ) has been repeatedly verified by numerous experimental characterizations of dislocations using commercially available indenters [8–10]. However, this picture is unlikely to hold when the indenter tip has an extraordinarily small size, such as a diameter less than ~20 nm. Recent atomistic simulations [11–13] and experimental results [14–16] suggest that the plastic zone then consists of prismatic dislocation loops (PDLs), propagating deep into the crystal. Compared with regular dislocations, dislocation loops (including both PDLs and helical loops) have some special characteristics. First, since the Burgers vector of a PDL is perpendicular to the loop plane, the size and slip path of a PDL are strongly confined by a prismatic slip tunnel. The PDL can only glide along one slip direction, as described by Ashby et al. [17]. Second, the glide of prismatic loops involves no dislocation intersection and reaction. Therefore, the stacked dislocation loop can preserve its configuration throughout the test and penetrate to a large depth below the surface. By contrast, regular dislocations can easily change their line length and slip plane by cross-slip, so that they spread as "flames" to form roughly a hemispherical distribution. The PDLs may thus lead to a distinctly different plastic zone, in terms of its make-up and morphology. There is a

* Corresponding authors.
E-mail addresses: dg_xie@xjtu.edu.cn (D.-G. Xie), zwshan@mail.xjtu.edu.cn (Z.-W. Shan).

https://doi.org/10.1016/j.actamat.2022.117944
1359-6454/

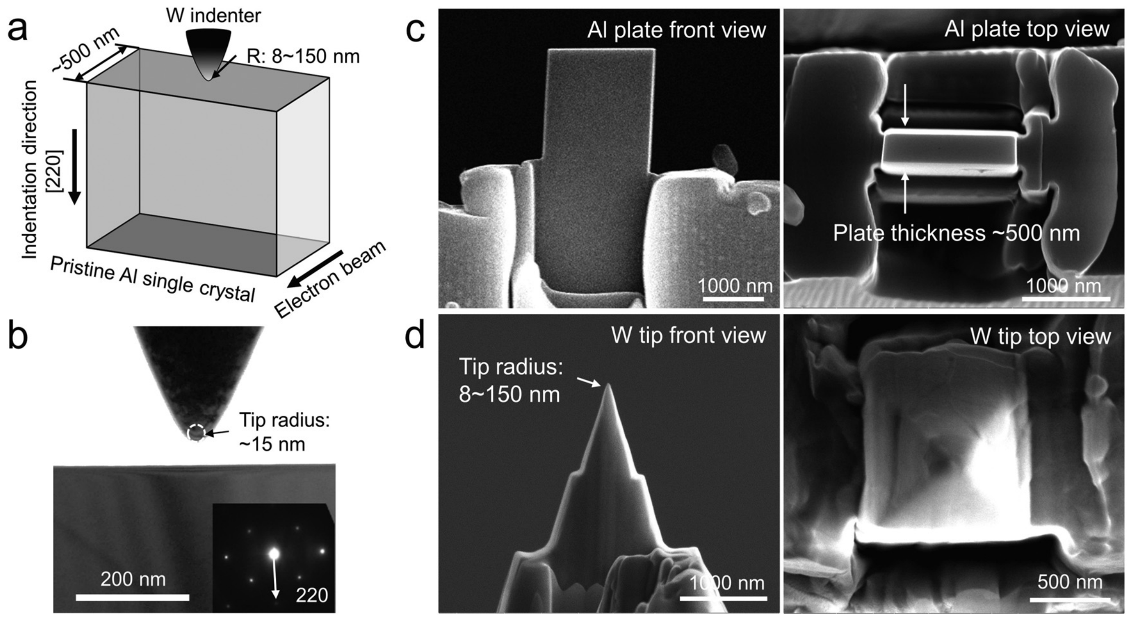

Fig. 1. The experimental setup for *in situ* nanoindentation. (a) Schematic illustration showing mechanical testing setup. (b) The bright field TEM image of the tungsten indenter and the single crystalline Al plate with nearly pristine interior. The inset is the diffraction pattern of the Al specimen ([002] zone axis and indention direction along [220]). (c) SEM images showing aluminum samples. Side view (left) and top view (right) of a typical Al plate. the plate thickness was measured to be ~500 nm. (d) SEM images showing side view (left) and top view (right) of a typical as-prepared tungsten tip, the FIB fabricated tip radius ranges from 8 to 150 nm.

pressing need to explore what happens in this case, especially for nanoscale mechanical tests such as in the atomic force microscopy (AFM) based nanoindentation [18–20]. An understanding of this scenario is also important for developing appropriate plastic mechanics models for nanoscale asperity contacts.

In situ testing inside a transmission electron microscope (TEM) is an informative technique to reveal the dislocation evolution during nanoindentation. To this end, previous experiments [15,16,21,22] have attempted the use of a nanoscale indenter, but the shape/size of the indenter tip was not well defined. Here we employ an *in situ* TEM nanoindentation experimental setup (Fig. 1), with indenter tips that have a well-defined spherical apex. The tip radius ranges from 8 to 150 nm, to cover the size regime of interest. Flat single crystalline aluminum plates offer ample sample volume to accommodate dislocation generation and propagation during nanoindentation. Moreover, to meet the "pristine crystal" assumption in the nanoindentation, the aluminum plates were well annealed to remove most, if not all, preexisting dislocations before engaging the tip, so that all the observed dislocations are freshly generated and their subsequent evolution is undisturbed by preexisting defects. In the following, we will show that the plastic zone transitions from 3D to 1D, depending on the contact diameter: when the contact diameters were larger than ~100 nm, a fully developed three-dimensional plastic zone (3D PZ) consisting of regular dislocations was observed. When the contact diameter was less than ~50 nm, we demonstrate a novel one-dimensional plastic zone (1D PZ) consisting of one single PDL array extending along the indentation direction up to 150 times of the indentation depth below the contact surface. In between these two sizes, the plastic zone is a mixture of the 1D and 3D types. Our results from molecular dynamics (MD) simulation further corroborate that the stress field generated by the indenter as well as other dislocations in the pile-up is a decisive factor in pushing the leading dislocations.

2. Experiments and methods

Sample preparation: A single crystal pure aluminum (99.9995%) disk was incised into 1.5 × 2 × 0.5 mm^3 rectangular plate, which was then mechanically polished to ~100 μm in thickness and electrochemically thinned to a few microns. After the thinning, the aluminum plates were attached to the sample holder using conductive epoxy with high-temperature compatibility. Before curing the epoxy, the orientation of the aluminum plates was carefully adjusted such that the indentation direction will be precisely aligned along [110] in the ensuing tests. Then, rectangular plates with thickness of ~500 nm were fabricated using focus ion beam (FEI Helios600), and the end surface was also polished flat with its normal aligned with the loading direction. Before nanoindentation tests, the aluminum plates were annealed at 400 °C for at least 30 min in vacuum to remove lattice defects and obtain an approximately pristine interior.

***In situ* TEM nanoindentation experiments**: The *in situ* TEM nanoindentation experiments were performed with Hysitron PI95 ECR Picoindenter in a JEM-2100F transmission electron microscope (operated at 200 kV). The indenters were made from a tungsten rod by using the focus ion beam to machine one end into a pyramidal tip with the spherical apex (radius=8 to 150 nm). We used displacement control at the loading rate of ~2 nm/s during indentation, and the resultant evolution of dislocation was recorded as movies with a Gatan 830 (SC200) CCD camera at frame rate = 10 fps.

Method of nanoindentation MD simulation: Atomic model of FCC Al with orientations — x: $[\bar{1}1\bar{2}]$, y: $[\bar{1}11]$, z: [110] — was constructed. The dimension of the model was 70.4 nm × 70.6 nm × 304.0 nm. The number of atoms was 91,387,224. The embedded atom method (EAM) potential for Al [23] was used to describe the interatomic interactions. The lattice constants and elastic constants were estimated as a = 4.05 Å, C_{11} = 114, C_{12} = 61.6, and C_{44} = 31.6 GPa, which agree with the experimentally determined values of a = 4.05 Å, C_{11} = 114, C_{12} = 61.9, and C_{44} = 31.6 GPa. Before starting indentation simulations, the models were first equilibrated using Parrinello-Rahman NPT ensemble method [24] for 50 ps at an in-plane normal stress of 0 Pa at simulation temperatures of 300 K to release the in-plane stresses. The z position of the spherical indenter with radius R_{sim} = 8 nm was controlled to move along an axis perpendicular to the model surface at 6 m/s. During the simulations, the center

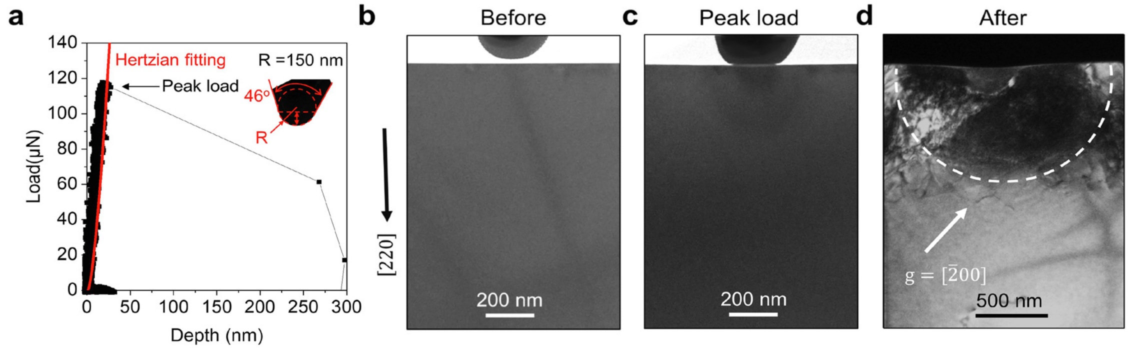

Fig. 2. Three-dimensional plastic zone (3D PZ) formed with the indenter tip radius of 150 nm. (a) The load-depth curve. The red line represents Hertzian fitting result. The upper right inset shows the TEM image of the indenter tip. (b) Bright-field image showing the dislocation structure before the indentation. (c) The frame extracted from indentation video at the peak load, as marked on the load-depth curve just before the pop-in, showing purely elastic response to the loading. (d) The dark-field image taken with [$\bar{2}$00] diffraction vector showing the dislocation structure after the indentation.

of mass of the atomic slab model was fixed and the x and y dimensions of the slab model were relaxed such that the normal stress was 0 Pa in these directions. The following repulsive force was assumed to act between the indenter and the slab model: $F(r_{sim}) = -K(r_{sim} - R_{sim})^2$; $r_{sim} < r_c$, where r_{sim} denotes the distance of the atoms in the target material to the centroid of the spherical indenter tip, K denotes a force constant, which was set to 10 eV/Å^3, and r_c denotes the potential cut-off distance, which was set to 0.63 nm.

3. Results and discussion

3.1. Three-dimensional plastic zone (3D PZ)

Fig. 2 and Movie S1 show the typical results from the *in situ* nanoindentation test with an indenter tip radius of 150 nm, which is valid down to a depth of ~105 nm, under displacement control mode at the loading rate of 2 nm/s. Fig. 2a is the quantitative data obtained during the nanoindentation, with the insert to show the initial shape of the indenter tip. The plot shows a clearly defined single pop-in event at the peak load of 118 μN with the indentation depth $h_{pop\text{-}in}$ of 21 nm. As shown in Fig. 2b, the plate has a "pristine crystal" interior and the indentation direction is along the [220] crystalline direction. Before the pop-in the whole sample remained pristine without generating any dislocations underneath the indenter, even at the peak load just before the pop-in (Fig. 2c). Assuming isotropic elasticity, the elastic contact between a rigid spherical indenter and a flat surface can be expressed by the well-known Hertzian contact model, the load P is related to indention depth h [25] by

$$P=\frac{4}{3}E^{*}R^{1/2}h^{3/2} \tag{1}$$

where R is the top radius of an indenter, E^* is the reduced elastic modulus which can be obtained from

$$\frac{1}{E^{*}} = \frac{1-\nu^2}{E} + \frac{1-\nu_i{}^2}{E_i} \tag{2}$$

where E_i is the indenter modulus and E is the specimen modulus. ν_i is the indenter Poisson's ratio and ν is the specimen Poisson's ratio.

The load-depth curve predicted by the Hertzian theory using the tip radius of 150 nm is also plotted in Fig. 2a with the red line. The experimental data fit well with the Hertzian model, indicating a purely elastic response before the pop-in event. Therefore, it is reasonable to apply the Hertzian elastic contact model to estimate the maximum shear stress underneath the indenter: $\tau_{max}=0.465P/(\pi R h_{pop\text{-}in})$, where P is the critical load and $h_{pop\text{-}in}$ is the critical indentation depth. By plugging measured values into the equation, we estimate the critical shear stresses for pop-in can reach 5.5 ± 0.8 GPa. The pop-in is accompanied by the generation of numerous regular dislocation lines underneath the indenter, expanding in various directions. Meanwhile, the indenter rushed downward to the displacement of 250 nm within approximately 5 ms (estimated from the data acquisition rate set at 200 points/second). Fig. 2d presents the dark-field postmortem characterization taken with [020] diffraction vector. A region of high-density dislocations was developed just below the contact location. We can observe that the dislocations are mainly contained in a hemispherical zone, as outlined in Fig. 2d. The hemispherical plastic zone confirms the picture of 3D PZ generated using commercially available indenters, as mentioned earlier. The radius of the zone of high-density dislocations is approximately 3 times larger than the residual indentation radius. This value is close to that proposed by Durst et al. [26], who empirically assumed the radius of the plastic zone should be 1.5 to 2.5 larger than the contact radius.

3.2. Three-dimensional plastic zone plus one-dimensional plastic zone (3D+1D PZ)

Using a smaller tip can result in the emission of dislocation loops. The high-density dislocation region is then accompanied by a long extending loop array. As shown in Fig. 3 and Movie S2, an indenter with the tip radius of ~25 nm (valid down to a depth of ~14 nm) was used to engage on the aluminum surface along the same crystallographic direction [220]. The corresponding quantitative mechanical data (p-h curve) is shown in Fig. 3a; only one yielding event can be clearly defined at the time t_p. Before the yielding point, we only observed an expanding semi-ellipse-shaped strain contour that expands with increasing load, indicating a purely elastic deformation without dislocation emission, and the applied load follows the Hertzian elastic curve. The stress drops at the peak load of 22 μN relate to the generation of abundant dislocations loops and regular dislocations (Fig. 3b). This peak load corresponds to the critical shear stress for yielding of 9.3 ± 2.0 GPa. Such a high stress is sufficient for the dislocation to nucleate homogeneously within the perfect lattice, although the effects of oxide film on the high stress could not be completely excluded. Unfortunately, at the high stresses the dislocation generation processes are too fast to be caught by the camera. The bright-field image of Fig. 3c clearly shows the distribution of the resultant dislocations. One single loop array extended to ~2.7 μm beneath the indenter, comprising of a coaxial stack of prismatic/helical dislocation loops led by two individual PDLs. Morphologically, such a long extending plastic zone consisting of dislocation loops has the appearance of a one-dimensional plastic zone (1D PZ). In addition to

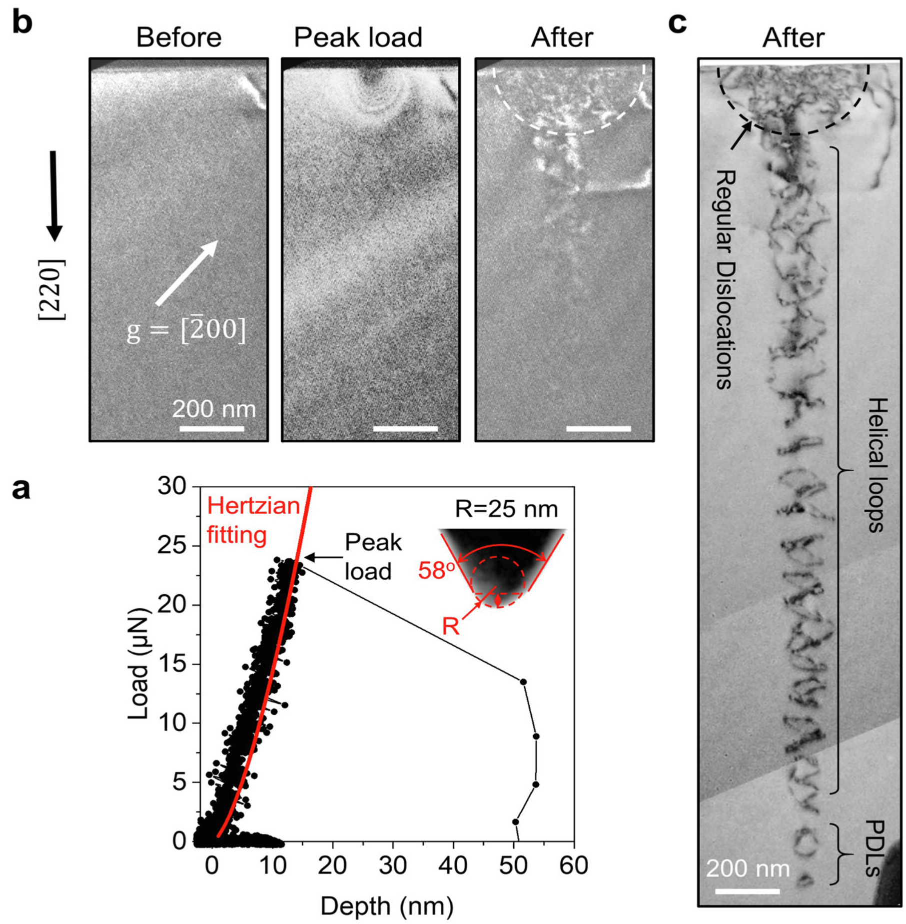

Fig. 3. Three-dimensional plastic zone plus one-dimensional plastic zone (3D+1D PZ) formed during *in situ* indentation with a tip of radius of 25 nm. (a) The load-depth curve, with the red line referring to the fitted curve using the Hertzian elastic model (b) Dark-field images taken with [$\bar{2}$00] diffraction vector showing the evolution of dislocation configuration with increasing indentation. The sample exhibited obvious elastic stress field contrast underneath the indenter at time t_p, corresponding to peak load as marked on the load-depth curve. (c) Bright-field image taken after indentation, showing dislocation configuration below the indent.

this, near the indented surface, there is also a hemispherical volume of jammed regular dislocations (3D PZ).

3.3. One-dimensional plastic zone (1D PZ)

With the indenter tip radius going further down, the indentation becomes more inclined to generate individual loops. The 1D PZ thus becomes dominating. Fig. 4 and Movie S3 show the results from such an indentation experiment using a tip with an apex radius of ~15 nm (valid depth for this measured radius is down to ~10 nm) and a corner angle of 60°. The *P-h* curve includes four displacement bursts, marked as P1-P4 in Fig. 4a. At the beginning of indentation, a nano-asperity on the indenter surface first contacted with the aluminum substrate, resulting in minor fluctuations just above the force noise floor in the load response. After that, the load increased elastically to about 7.5 μN (indentation depth = 8 nm), followed by a major pop-in. In the ensuing loading, two other pop-in events happened, as indicated in Fig. 4a.

By correlating these displacement bursts with the microstructural evolution in the movie, as shown in Fig. 4c-d, the first two displacement bursts (P1-P2) can be related to the generation of PDLs that pile up in a row along [220], which is the slip direction of dislocations in aluminum, while in the third displacement burst P3, a few loops are emitted first and then some regular dislocations follow, and the ensuing fourth displacement burst (P4) only generates regular dislocations. Fig. 4d shows a full picture of dislocations remaining under the indenter after indentation. There are three different types of dislocations, *i.e.* the PDLs mainly in the form of single loops, the helical loops with each one involving two or more loops, and the regular dislocations. These different dislocations are generated through transition stages: in the middle of P3, the individual PDLs first transition to helical dislocations, which further transition to regular dislocations at the end of P3. As shown in Fig. 4d, the leading loop slips to a depth of 3400 nm before the gliding stops, even though the indentation depth is as small as 22 nm at the moment of P3. The penetration depth is 150 times the indentation depth, and thus far beyond the prediction by the Nix-Gao model, where all the generated dislocations are contained in a hemisphere with a radius comparable to the indent radius [8,9,27]. The behavior of PDLs has been hypothesized before and has also been observed in some other types of experiments, such as the growth of a spherical particle in a solid matrix [28,29]. However, ours is the first time to directly observe what actually happens underneath a nanoindenter. The one published by Lee et al. [16] used an inverse indenter rather than a normal indenter tip.

3.4. Configuration of the one-dimensional loop array

In a PDL array, the position of a loop is determined by the equilibrium between the repulsive force exerted by other loops and the lattice friction. The repulsive force between loops (P_{rz}) is short-ranged [30], decreasing fast with the inter-loop spacing z following the relation $P_{rz} = br^3G/(1-\nu)z^4$, where G is the shear modulus, b

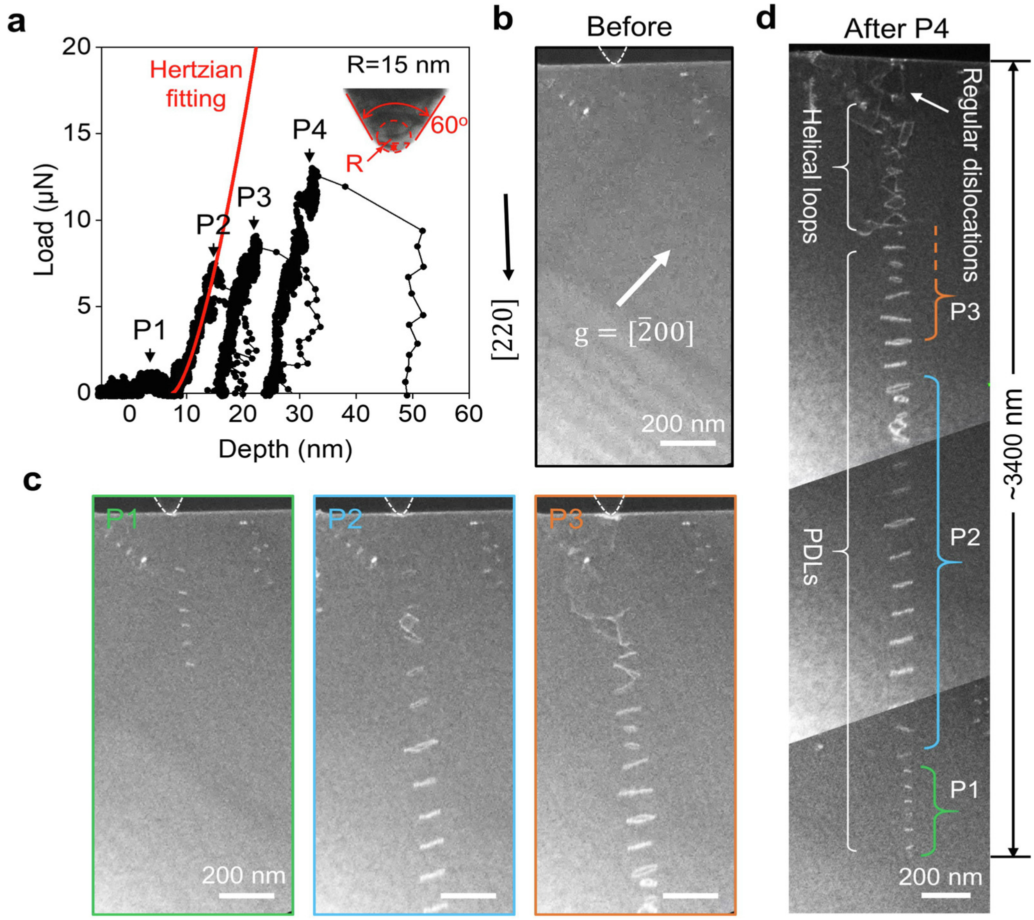

Fig. 4. The formation of one-dimensional plastic zone (1D PZ) during *in situ* indentation with a tip radius of 15 nm. (a) The load-depth curve, with the red line referring to the fitted curve using the Hertzian elastic model. Four yielding events are indicated by arrows P1 to P4. (b) The dark-field images taken with $[\bar{2}00]$ diffraction vector, showing the interior structure before the indentation. (c) Dark-field images of the dislocation configuration after each corresponding yielding event as indicated at the depth-load curve; the diffraction vector is $[\bar{2}00]$. (d) Overview image stitched together using four images, showing the dislocation structure below the indenter after indentation.

is the magnitude of the Burgers vector, r is the loop radius, and ν is Poisson's ratio. The experimental observations indicate that the spacing between loops is comparable with their diameters. Consequently, the repulsive force that a loop feels from the loops farther than its third neighbor is almost negligible (the repulsive force from the first and second neighbors accounts for 94% of the sum). This means that the spacing between two loops is largely dictated by the nearest two or three loops. Another conclusion from the above analysis is that when the glide of a dislocation loop in an array is driven by the elastic stress field of the previous one, dislocation motion can be easily transferred onwards. Specifically, when a new dislocation loop is emitted from the indentation site and squeezed into the row, a net repulsive stress between loops will be generated to push the nearest loop forward, which in the same way continues to push the next one. This action is repeated like a moving wave that propagates from the tail of the loop array to the leading loop. In this way, although the indentation stress field only provides a high driving stress in a small hemispherical volume, the plasticity can be transmitted over a long distance, enabled by the re-lay of dislocation loops constituting the array. Therefore, although the elastic stress field imposed by the indenter is only able to drive regular dislocations to a distance comparable to the contact size, the glide of dislocation loops in an array can be sustained over a long distance. This explains our observation that the dislocation loops marched on like a group towards the deep interior of the aluminum crystal. Also derived from the force-chain mechanism is that the high stress around the indenter is not sustained unless/until the movement of the loop array is blocked by obstacles or heterogeneous dislocation nucleation sets in.

Moreover, the lattice friction stress (τ_0) can be extracted from the equilibrium configuration of PDLs. Xin et al. suggested that the configuration of the loop array is determined by the balance between the repulsive interaction between loops and the lattice friction stress (τ_0) opposing dislocation movement [31]. For an array of $N+1$ coaxial dislocation loops with diameter d, the first leading loop is numbered 0 and the following loops is numbered $i = 1 \sim N$ (Fig. 5a). If we define a normalized loop position:$\zeta_i = (\Delta Z_i)/d(i = 1 \sim N)\zeta_i = (\Delta Z_i)/d(i = 1 \sim N)$, where ΔZ_i represents the distance between loop i and the loop 0 . When the loop distance is large relative to the loop size, ζ_i can also be expressed as follow:

$$\zeta_i = \left(\frac{3\pi}{4\bar{d}}\right)^{\frac{1}{4}} \left\{ \begin{array}{l} \frac{4}{3}\left[N^{3/4} - (N+1-i)^{3/4}\right] + \frac{1}{2}\left[N^{-1/4} + (N+1-i)^{-1/4}\right] \\ \quad + \frac{1}{48}\left[(N+1-i)^{-5/4} - N^{-5/4} +\right] \end{array} \right\} \tag{3}$$

where the scaled loop size:

$$\bar{d} = 2\pi(1-\nu)\tau_0 d/Gb \tag{4}$$

For the three sets of loop arrays with their average loop diameter of 33 nm, 60 nm, and 30 nm, respectively, the normalized loop position between each loop and the corresponding loop 0 was measured, as shown in Fig. 5b. We can then fit Eq. (3) for the measured loop positions, to obtain the scaled loop size $\bar{d}$. By insert-

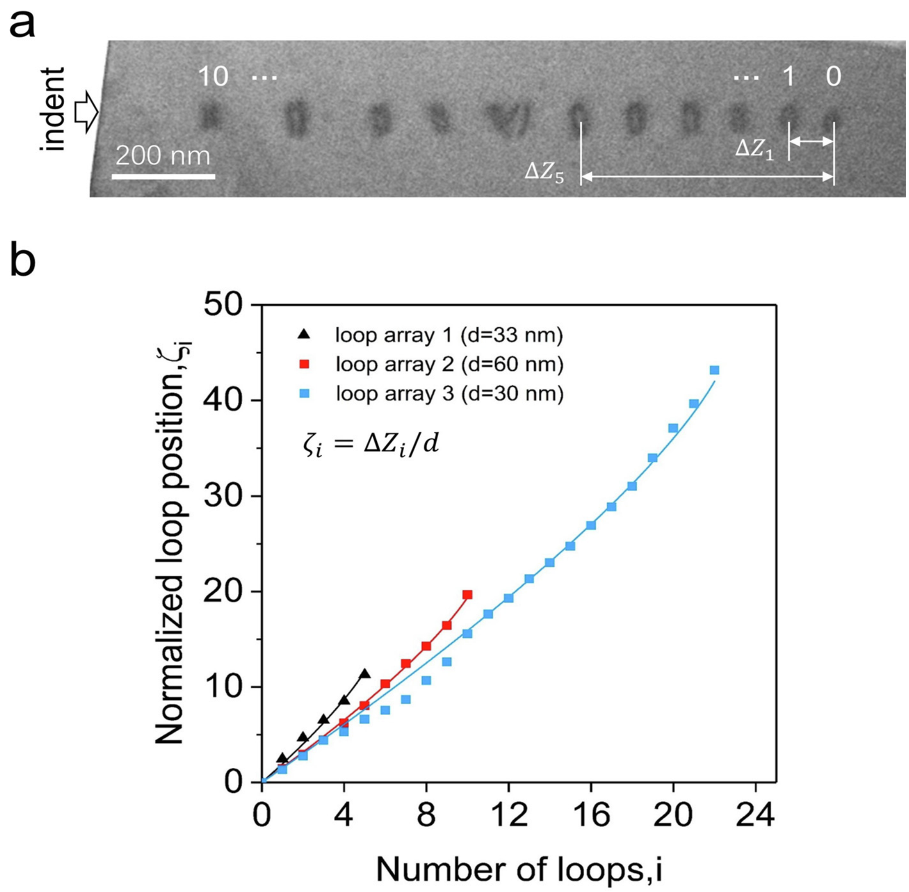

Fig. 5. Configuration of coaxial prismatic dislocation loops and the fitting results. (a) TEM image of a set of PDLs in an array, ζ_i is used to represent the position of loop i from the first leading loop (normalized by average loop diameter d). (b) the normalized loop position for each PDL. The lines represent the fitting results using the Eq. (1).

ing reasonable parameters for aluminum ($\nu = 0.35$, $G = 26$ GPa, and $b = 0.28$nm) into Eq. (4), the lattice friction stress τ_0 can thus be calculated as 1.22, 1.11 and 0.94 MPa for the three loop arrays, respectively. Therefore, the averaged friction stress $\tau_0 = 1.10 \pm 0.14$ MPa, close to the estimated value for edge dislocations in Al by atomistic simulation (~ 1 MPa [32], 1.6 MPa [33]) and mechanical tests (0.78 MPa [34], 1.05 MPa [35]).

3.5. Size-dependent transition of plastic zones

Obviously, the transition of the plastic zone morphology is rooted in the size-dependent transition of self-closed loops to regular dislocations. In order to reveal the relation between contact sizes and dislocation types, the contact diameters and loop diameters are measured from the *in situ* video frames immediately after yielding events in several indentation tests with various indenter tip radii, assuming the measurement errors as 1~2 pixels. The results are plotted as Fig. 6, which demonstrates that the loop size is nearly proportional to the contact diameter, by a factor of ~1.2. Besides, there are two threshold contact diameters, with D_{c1}=~50 nm denoting the transition from the emission of PDLs to the generation of helices, and D_{c2}=~100 nm for a transition between loop generation and nucleation of regular dislocations.

To explain the above two transitions from singular PDLs to helical loops to regular dislocations, we first need to understand the mechanism of nucleating a PDL. Previous research has observed the generation of PDL near a precipitation particle growing from a ductile metal matrix [17], which is supposed to be similar to the scenario in nanoindentation (the schematic diagram of this process is shown in Figure S5). The underlying mechanism of PDL nucle-

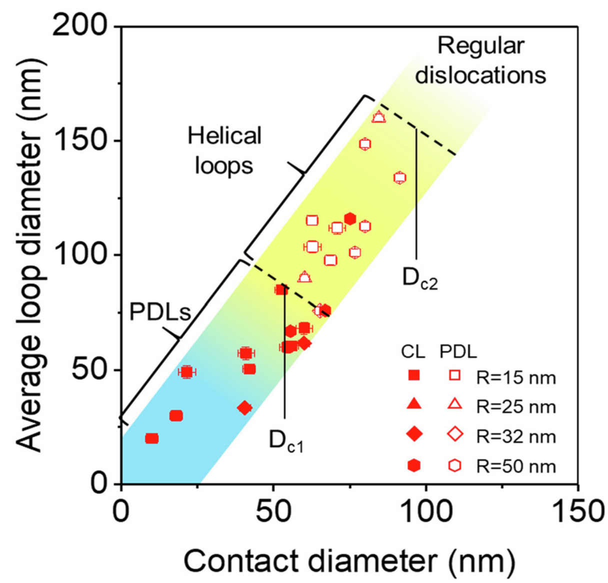

Fig. 6. The relationship between the indent contact radius and loop radius/types. The size of the points represents the initial indenter tip radius. When the contact diameter is smaller than ~50 nm, PDLs are favorable; closed helical loops are more favorable otherwise. The indent contact radius is measured directly from *in situ* video frames just before the yielding events.

ation during nanoindentation has also been studied by molecular dynamics (MD) simulations [13,36,37]. A well-accepted model suggests that due to the stress generated around the contact interface,

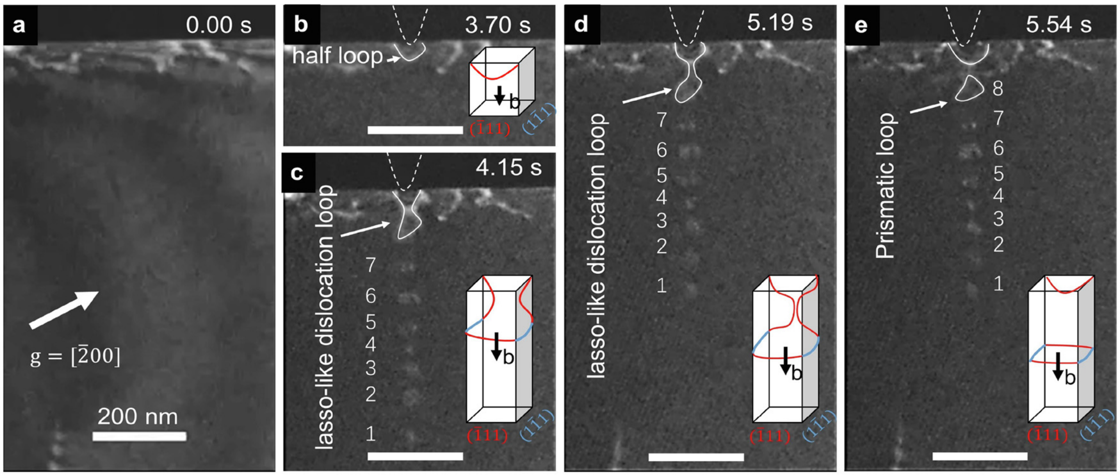

Fig. 7. The formation process of an individual PDL. (a) Dark-field TEM image of the single crystal Al plate before the indentation. (b) The nucleation of a half loop underneath the indenter, indicated by a white arrow. (c-d) Formation of a lasso-like dislocation loop attached to the half loop. (e). A new PDL is released when the two dislocation segments meet and react. Insets in c-e schematically illustrate the dislocation shapes in the corresponding images, compared with the glide prism bounded by four {111} planes. All scale bars represent 200 nm.

a shear loop will nucleate first and bulge out on the {111} plane in response to the indentation stress field, when the shear stress is greatest on the adjacent {111} planes, the first cross-slip occurs. In the same way, the second cross-slip event occurs, bringing the segments back to the original slip plane. The lasso-like dislocation loop with three sides of a parallelogram and a neck is generated from those two steps of cross slip processes. During the following slip, the screw segments of this neck attract and annihilate each other, resulting in the birth of an individual PDL. Despite multiple atomistic modeling to show this process [12,36-39], an experimental demonstration is still lacking. In another nanoindentation experiment, we also observed a similar process showing how an individual dislocation loop is generated near the contact interface. In Fig. 7 and Movie S4, the generation of a PDL can be divided into four transient states. In the beginning, a half loop is nucleated from the contact interface and bows out in a (111) plane along the direction of [220] (Fig. 7b). In the following short period of 0.45 s, this half loop acts as an embryonic dislocation source from which seven PDLs are nucleated and injected into the crystal, a process too fast to be observed clearly. After the emission of these loops, most of the stored elastic energy has been exhausted, and the dislocation nucleation process slowed down, thus allowing for catching some details of the next nucleation event. As shown in Fig. 7c, the half loop developed into a lasso-like dislocation loop near the indenter. The neck of this lasso-like dislocation loop became increasingly narrower with the rising load, until it shrank to a point and the dislocation segment under the neck pinched off to form an individual PDL (Fig. 7d-e).

It is noteworthy that multiple cross-slips and the reaction of shear dislocation segments are involved in the generation of a PDL, and both processes are highly sensitive to the local stress field. Therefore, we suggest that our observed transitions of dislocation configuration must be related to the effect of local stress field on dislocation nucleation. The formation of a closed prismatic loop depends on the symmetry of the indentation stress field. The simulation result shows that the cross slip occurs exactly where the force condition changes [36,40]. Therefore, the symmetry of the indentation stress field ensures that the two cross-slipped screw segments meet each other on the same slip plane, which is the mechanism for the loop to pinch off. If they miss each other, a helical loop will be generated. From this point of view, the generation of the individual closed loop is sensitive to the local stress fluctuations. After the pinching-off of PDL, the stress relaxes and the shear loop retracts back, returning to a pristine state in the indent region. As the indentation proceeds, those PDL nucleation processes repeat. With the increase of contact area, to accommodate the lateral strain, the dislocations nucleation and propagation are also activated in the other two <220> directions. The intersection of the propagating directions provides the chances for the dislocations to meet and interact with each other, resulting in tangles or locks that reduce the dislocation mobility. The presence of dislocation near the contact interface can disturb the nucleation of dislocation loops, by changing the local elastic stress field to interrupt the closing-up of a loop or intermittently reacting with nucleated loops, thus leading to the creation of helical loops. As an increasing number of dislocations jam up near the contact area, the formation of individual dislocation loops finally becomes statistically impossible, and in the later stage, dislocation forest and mutual dislocation interactions (such as Frank–Read sources [12], dislocation unjamming [41,42]) are presumed to be the dominant mechanism of plasticity. This transition process has also been observed in our own atomistic simulations: we conducted a MD nanoindentation simulation on a (110) surface of cuboid-shaped Al atomistic model using 8 nm radius spherical indenter as shown in Fig. 8. The dislocation behavior during the nanoindentation simulation is recorded as a movie (Movie S5). It can be seen that with the expansion of the contact area and plastic zone, the structure of nucleated dislocations becomes more and more complex. Furthermore, the distributions of resolved shear stress on the $(1\bar{1}1)[110]$ slip system at the elastic and PDL emission stages (Fig. 9a,b) were symmetric, while those after the helical loop emission stage (Fig. 9c,d) lose such symmetry, and thus the distributions clearly illustrate the break-down of the symmetry of the indentation stress field at the generation of helical loops.

This picture of the dislocation evolution process has no significant anisotropic effects. When we change to another indentation direction was off $[\bar{1}\bar{1}1]$ by about 10°, we observed a similar dislocation evolution process, as shown in Fig. 10 and Movie S6. During this indentation experiment, only one long PDL array was punched into the crystal, and extended along $[02\bar{2}]$ direction that has the largest Schmidt factor to the indentation direction among all the three possible <110> directions, while in the other two possible glide directions ($[\bar{2}\bar{2}0]$ and $[\bar{2}02]$), we only observed a few tiny loops at the early stage and further dislocation nucleation was suppressed due to the strain relaxation effect from the dislocation nucleation along the preferred direction. In addition,

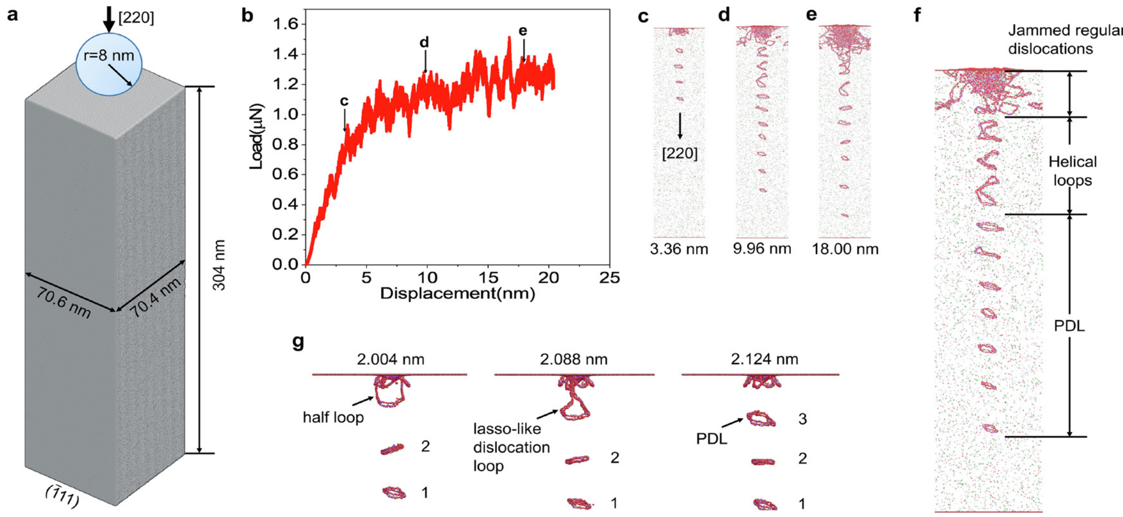

Fig. 8. MD-simulated dislocation generation, during nanoindentation using an 8-nm radius sphere on aluminum along [220] direction. (a) Simulation model. (b) Load-displacement curve. (c-e) Snapshots of at different stages of the nanoindentation depth. Dislocations are detected by central symmetry parameter coloring. (f) The overview image of emitted dislocations. (g) The simulated formation process of a PDL.

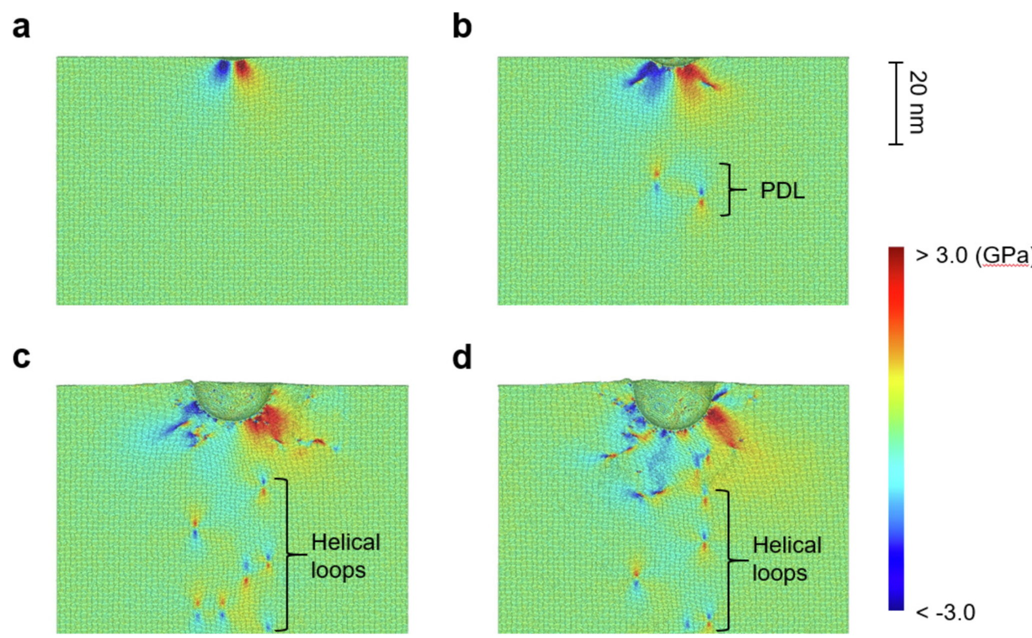

Fig. 9. The distributions of resolved shear stress on the $(1\bar{1}1)[110]$ slip system during nanoindentation MD simulation with an indenter radius of 8 nm. (a) The elastic stage before dislocation generation. (b) The PDL emission stage. (c) The helical loop emission stage. (d) The regular dislocation generation stage.

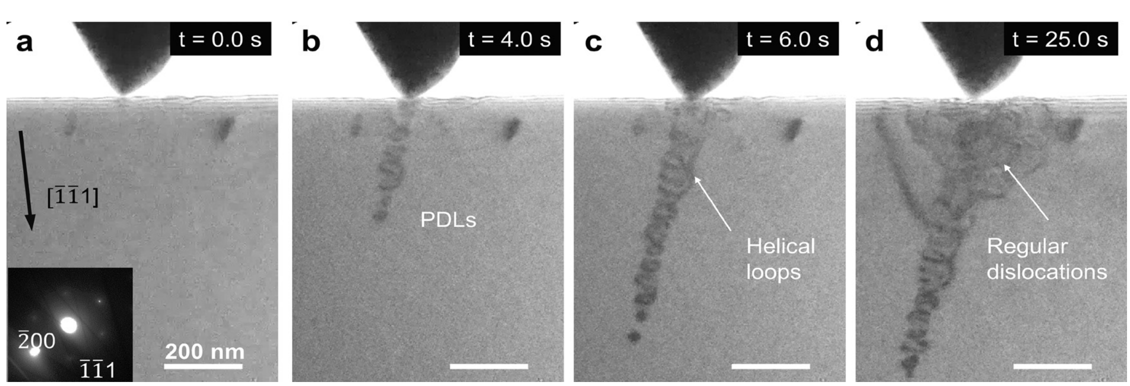

Fig. 10. The evolution of dislocation configuration when an indentation is made along the $[\bar{1}\bar{1}1]$ direction of aluminum crystal. (a) Image showing the indenter and aluminum sample before engaging the tip. (b-d) The image series showing dislocation structure at different moments of indentation. Time labels are at the top of each image.

even if dislocation loops were generated along the other two directions, they will meet and escape at the free surfaces after travelling a short distance after emission, and thus can only form a short array of loops. As the contact radius increases, the transitions from individual PDLs to helical PDLs to jammed regular dislocation lines were also observed, similar to the observation in indentations along [220] direction.

Previous theories and experimental characterizations show a consensus that the indentation only creates dislocations spreading in three dimensions, even in the early stage of the indentation [8,21,43]. What is more, in order to measure intrinsic film properties, a currently well-recognized empirical rule is that the indentation penetration depth must be less than 10% of the film thickness [44]. However, as we have observed, the plastic zone can extend in one dimension to a distance of several micrometers, realized by the fast glide of an array of small PDLs in the direction of their Burgers vector, even though the indentation depth is only ~20 nanometers. This unusual penetration ability of the dislocation arrays is of significance for thin-film mechanical testing, considering that significant back stress can be built up to induce hardening when the movement of PDLs is impeded by substrate/film interface or some other obstacles. Our finding is even more important for applications using the atomic force microscope (AFM) with a tip radius of only a few nanometers [45,46] because such an extraordinarily sharp indenter tip would generate PDLs, which have a high propensity to glide a large distance before piling up at obstacles.

In the following, we define a penetration ability factor for dislocations, *f*. For an array of dislocation loops, the penetration ability factor is evaluated as the distance from the first leading loop to the indented site divided by the indentation depth (solid circles in Fig. 11). For the regular dislocations residing in a hemispherical zone, we use the ratio between the fitted radius of this hemisphere and the indentation depth to represent the propagation ability factor (hollow circles in Fig. 11). In Fig. 11 we summarized the results from a few indentation tests with tips of varying radius, to show the propagation ability factor for dislocations generated from different contact diameters in pop-in events. When the contact radius before yielding is smaller than ~80 nm, we observed that the PDLs array could extend over one hundred times deeper than the penetration depth of the indenter, also ten times deeper than that predicted by the 10% empirical rule mentioned above [47]. However, for regular dislocations, the propagation ability factors are about ten. With the increase of the contact diameter, the regular dislocations would expand and gradually overwhelm the PDLs, which have stopped moving after the first few pop-ins. When the contact radius before yielding is larger than ~100 nm, most of the dislocations generated during the indentation would be contained in a hemispherical volume with a radius ten times the indentation depth. This indicates that the 10% empirical criterion is only valid for indentations using a relatively large indenter, or when the contact diameter significantly exceeds ~100 nm.

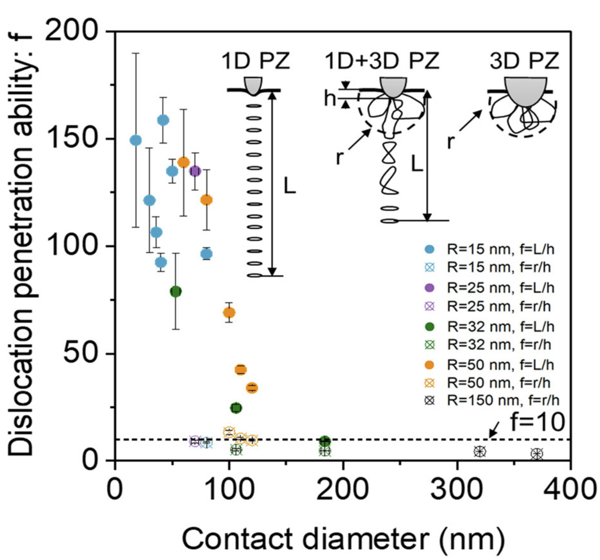

Fig. 11. Dislocation penetration ability *f* versus the contact area. Here the dislocation penetration ability factor, as shown in the inset: is evaluated using $f = L/h$ for PDLs/helices (solid circles), and $f = r/h$ for jammed regular dislocations (hollow circles), where L, r and h are marked in the inset.

4. Summary

Our work raises several points that are worthy of attention and have potential impact. First, we note the observed early-stage plasticity induced by nanoscale contact is in fact a common occurrence, considering that commercially available nanoindentation tips usually start with an apex/asperity radius of a few tens of nanometers, let alone the much sharper tips used in AFM. Our observations therefore offer a new perspective into what could happen using the popular nanoindentation methodology. Second, our results shed new light on the indenter size effect, specifically on the form of indentation plastic zone, bridging previous predictions from atomistic simulations with experimental observations. Third, we found that the dislocation loops in the array can be pushed to travel a long distance. The probability for them to meet other preexisting obstacles and thus cause hardening is much higher than that expected from regular dislocations. This would be especially important for mechanical measurements on films with a thickness of a few micrometers or less, because the dislocation loops have the ability to reach and interact with the film/matrix interface, thus altering the properties being examined. One can observe abnormal size effects at very shallow indentation depth, effects that are not taken into account in the Nix-Gao model. Fourth, our experimental method provides a novel way to “focus” defects so as to interrogate their interactions, for example, by impinging PDLs onto preexisting grain boundaries, phase boundaries or precipitate particles. One can also envision the use of a sharp indenter to implant dislocation loop arrays at desired places, one location at a time, setting up a grid pattern of obstacles to moving dislocations in the film for strengthening or other purposes: *e.g.* to pattern self-assembled low-dimensional nanostructures [27,48]

Author contributions

Z.S. supervised the project., Z.N., and D. X. designed the experiments. Z.N. conducted the experimental work. S.O. guided the MD modeling analysis. Y.S. conducted the MD simulations. Z.N., D.X., Z.S., and E.M. wrote the paper. All authors contributed to the discussions of the results.

Declaration of Competing Interest

The authors declare that they have no known competing financial interests or personal relationships that could have appeared to influence the work reported in this paper.

Acknowledgments

The authors acknowledge the supports from Natural Science Foundation of China (52031011, 51971169). We also appreciate the support from the International Joint Laboratory for Micro/Nano Manufacturing and Measurement Technologies and the Collaborative Innovation Center of High-End Manufacturing Equipment. Y.S.

and S.O. acknowledge the Center for Computational Materials Science, IMR, Tohoku University for the use of MASAMUNE-IMR and the Cybermedia Center, Osaka University for the use of OCTOPUS. S.O. acknowledges the support by the JSPS KAKENHI Grant Nos. JP17H01238 and JP17K18827. We acknowledge P. Zhang, C. Y. B. Qin (Xi'an Jiaotong University) for assistance in focused ion beam and TEM experiments.

Supplementary materials

Supplementary material associated with this article can be found, in the online version, at doi:10.1016/j.actamat.2022.117944.

References

[1] T. Zhu, J. Li, Ultra-strength materials, Prog. Mater Sci. 55 (7) (2010) 710–757.
[2] L.Y. Chen, M.R. He, J. Shin, G. Richter, D.S. Gianola, Measuring surface dislocation nucleation in defect-scarce nanostructures, Nat. Mater. 14 (7) (2015) 707–713.
[3] T.A. Michalske, J.E. Houston, Dislocation nucleation at nano-scale mechanical contacts, Acta Mater. 46 (2) (1998) 391–396.
[4] D. Lorenz, A. Zeckzer, U. Hilpert, P. Grau, H. Johansen, H.S. Leipner, Pop-in effect as homogeneous nucleation of dislocations during nanoindentation, Phys. Rev. B 67 (17) (2003).
[5] C.A. Schuh, J.K. Mason, A.C. Lund, Quantitative insight into dislocation nucleation from high-temperature nanoindentation experiments, Nat. Mater. 4 (8) (2005) 617–621.
[6] Y. Sato, S. Shinzato, T. Ohmura, T. Hatano, S. Ogata, Unique universal scaling in nanoindentation pop-ins, Nat. Commun. 11 (1) (2020) 4177.
[7] W.D. Nix, H. Gao, Indentation size effects in crystalline materials: a law for strain gradient plasticity, J. Mech. Phys. Solids 46 (3) (1998) 411–425.
[8] Y.L. Chiu, A.H.W. Ngan, A TEM investigation on indentation plastic zones in Ni3Al(Cr,B) single crystals, Acta Mater. 50 (2002) 2677–2691.
[9] L. Zhang, T. Ohmura, Plasticity initiation and evolution during nanoindentation of an iron-3% silicon crystal, Phys. Rev. Lett. 112 (14) (2014) 145504.
[10] C.F. Robertson, M.C. Fivel, A study of the submicron indent-induced plastic deformation, J. Mater. Res. 14 (6) (1999) 2251–2258.
[11] T. Tsuru, Y. Shibutani, Anisotropic effects in elastic and incipient plastic deformation under (001), (110), and (111) nanoindentation of Al and Cu, Phys. Rev. B 75 (3) (2007).
[12] J. Li, K.J. Van Vliet, T. Zhu, S. Yip, S. Suresh, Atomistic mechanisms governing elastic limit and incipient plasticity in crystals, Nature 418 (6895) (2002) 307–310.
[13] S. Jiao, W. Tu, P. Zhang, W. Zhang, L. Qin, Z. Sun, J. Chen, Atomistic insights into the prismatic dislocation loop on Al (1 0 0) during nanoindentation investigated by molecular dynamics, Comput. Mater. Sci. 143 (2018) 384–390.
[14] S. Graça, P.A. Carvalho, R. Colaço, Dislocation structures in nanoindented ductile metals—a transmission electron microscopy direct observation, J. Phys. D Appl. Phys. 44 (33) (2011) 335402.
[15] A. Minor, J. Morris Jr, E. Stach, Quantitative *in situ* nanoindentation in an electron microscope, Appl. Phys. Lett. 79 (11) (2001) 1625–1627.
[16] S. Lee, A. Vaid, J. Im, B. Kim, A. Prakash, J. Guenole, D. Kiener, E. Bitzek, S.H. Oh, In-situ observation of the initiation of plasticity by nucleation of prismatic dislocation loops, Nat. Commun. 11 (1) (2020) 2367.
[17] M.F. Ashby, L. Johnson, On the generation of dislocations at misfitting particles in a ductile matrix, Philos. Mag. 20 (167) (1969) 1009–1022.
[18] T. Filleter, R. Bennewitz, Nanometre-scale plasticity of Cu(100), Nanotechnology 18 (4) (2007) 044004.
[19] M. Dupraz, G. Beutier, T.W. Cornelius, G. Parry, Z. Ren, S. Labat, M.I. Richard, G.A. Chahine, O. Kovalenko, M. De Boissieu, E. Rabkin, M. Verdier, O. Thomas, 3D Imaging of a dislocation loop at the onset of plasticity in an indented nanocrystal, Nano Lett. 17 (11) (2017) 6696–6701.
[20] Y. Gaillard, C. Tromas, J. Woirgard, Study of the dislocation structure involved in a nanoindentation test by atomic force microscopy and controlled chemical etching, Acta Mater. 51 (2003) 1059–1065.
[21] A.M. Minor, E.T. Lilleodden, E.A. Stach, J.W. Morris, Direct observations of incipient plasticity during nanoindentation of Al, J. Mater. Res. 19 (01) (2011) 176–182.
[22] A.M. Minor, S.A. Asif, Z. Shan, E.A. Stach, E. Cyrankowski, T.J. Wyrobek, O.L. Warren, A new view of the onset of plasticity during the nanoindentation of aluminium, Nat. Mater. 5 (9) (2006) 697–702.
[23] Y. Mishin, D. Farkas, M.J. Mehl, D.A. Papaconstantopoulos, Interatomic potentials for monoatomic metals from experimental data and ab initio calculations, Phys. Rev. B 59 (5) (1999) 3393–3407.
[24] M. Parrinello, A. Rahman, Crystal structure and pair potentials: a molecular–dynamics study, Phys. Rev. Lett. 45 (14) (1980) 1196–1199.
[25] K.L. Johnson, Contact mechanics, J. Tribol. 108 (4) (1985) 464.
[26] K. Durst, B. Backes, M. Göken, Indentation size effect in metallic materials: correcting for the size of the plastic zone, Scr. Mater. 52 (11) (2005) 1093–1097.
[27] C.R. Taylor, E.A. Stach, G. Salamo, A.P. Malshe, Nanoscale dislocation patterning by ultralow load indentation, Appl. Phys. Lett. 87 (7) (2005) 073108.
[28] A. Eikum, G. Thomas, Precipitation and dislocation nucleation in quench-aged Al-Mg alloys, Acta Metall. 12 (5) (1963) 537–545.
[29] R.S. Barnes, D.J. Mazey, Stress-generated prismatic dislocation loops in quenched copper, Acta Metall. 11 (4) (1963) 281–286.
[30] R. Bullough, R.C. Newman, The spacing of prismatic dislocation loops, Philos. Mag. 5 (57) (1960) 921–926.
[31] X.J. Xin, G.S. Daehn, R.H. Wagoner, Equilibrium configuration of coaxial prismatic dislocation loops and related size-dependent plasticity, Acta Mater. 45 (5) (1997) 1821–1836.
[32] S.G. Srinivasan, X.Z. Liao, M.I. Baskes, R.J. McCabe, Y.H. Zhao, Y.T. Zhu, Compact and dissociated dislocations in aluminum: implications for deformation, Phys. Rev. Lett. 94 (12) (2005) 125502.
[33] I. Shin, E.A. Carter, Possible origin of the discrepancy in Peierls stresses of fcc metals: first-principles simulations of dislocation mobility in aluminum, Phys. Rev. B 88 (6) (2013).
[34] T. Kosugi, T. Kino, A new internal friction peak and the problem of the Peierls potential in f.c.c. metals, Mater. Sci. Eng. A 164 (1–2) (1993) 368–372.
[35] J.N. Wang, Prediction of Peierls stresses for different crystals, Mater. Sci. Eng. A 206 (1996) 259–269.
[36] J. Gagel, D. Weygand, P. Gumbsch, Formation of extended prismatic dislocation structures under indentation, Acta Mater. 111 (2016) 399–406.
[37] T.P. Remington, C.J. Ruestes, E.M. Bringa, B.A. Remington, C.H. Lu, B. Kad, M.A. Meyers, Plastic deformation in nanoindentation of tantalum: a new mechanism for prismatic loop formation, Acta Mater. 78 (2014) 378–393.
[38] F. Seitz, Prismatic dislocations and prismatic punching in crystals, Phys. Rev. 79 (4) (1950) 723–724.
[39] Y. Shibutani, T. Tsuru, A. Koyama, Nanoplastic deformation of nanoindentation: crystallographic dependence of displacement bursts, Acta Mater. 55 (5) (2007) 1813–1822.
[40] H. Yu, A.C.F. Cocks, E. Tarleton, Formation of prismatic dislocation loops during unloading in nanoindentation, Scr. Mater. 189 (2020) 112–116.
[41] F.F. Csikor, C. Motz, D. Weygand, M. Zaiser, S. Zapperi, Dislocation avalanches, strain bursts, and the problem of plastic forming at the micrometer scale, Science 318 (5848) (2007) 251–254.
[42] P.D. Ispanovity, L. Laurson, M. Zaiser, I. Groma, S. Zapperi, M.J. Alava, Avalanches in 2D dislocation systems: plastic yielding is not depinning, Phys. Rev. Lett. 112 (23) (2014) 235501.
[43] W. Zielinski, H. Huang, W.W. Gerberich, Microscopy and microindentation mechanics of single crystal Fe−3wt.% Si: part II. TEM of the indentation plastic zone, J. Mater. Res. 8 (6) (1993) 1300–1310.
[44] H.B.X. Cai, Hardness measurements of thin films-determining depth to thickness using FEM, Thin Solid Films 264 (1995) 59–71.
[45] B. Bhushan, V.N. Koinkar, Nanoindentation hardness measurements using atomic force microscopy, Appl. Phys. Lett. 64 (13) (1994) 1653–1655.
[46] B.R. Neugirg, S.R. Koebley, H.C. Schniepp, A. Fery, AFM-based mechanical characterization of single nanofibres, Nanoscale 8 (16) (2016) 8414–8426.
[47] R. Saha, W.D. Nix, Effects of the substrate on the determination of thin film mechanical properties by nanoindentation, Acta Mater. 50 (1) (2002) 23–38.
[48] K.M. Atsutomo Nakamura, Jun Tohma, Takahisa Yamamoto, Yuichi Ikuhara, Conducting nanowires in insulating ceramics, Nat. Mater. 2 (2003) 453–456.